Polymer 51 (2010) 4686–4697

Contents lists available at ScienceDirect

Polymer

journal homepage: www.elsevier.com/locate/polymer

Polyethylene/palygorskite nanocomposites: Preparation by *in situ* polymerization and their characterization

Wei Li [a], Alina Adams [b,*], Jingdai Wang [a,**], Bernhard Blümich [b], Yongrong Yang [a]

[a] State Key Laboratory of Chemical Engineering, Department of Chemical Engineering, Zhejiang University, Hangzhou 310027, PR China
[b] Institut für Technische Chemie und Makromolekulare Chemie, RWTH Aachen University, Templergraben 55, D-52056 Aachen, Germany

ARTICLE INFO

Article history:
Received 19 May 2010
Received in revised form
12 August 2010
Accepted 13 August 2010
Available online 26 August 2010

Keywords:
Polyethylene
Palygorskite
Nanocomposites

ABSTRACT

A naturally occurring clay mineral, palygorskite, which has the microstructure of nano-fibers, was used to support a metallocene compound, Cp_2TiCl_2. After activation by methylaluminoxane, the supported catalyst initiated an *in situ* ethylene polymerization resulting in the exfoliated dispersion of the nano-fibers into the polyethylene matrix. With no further chemical modification of the palygorskite after thermal treatment, the activity of the supported catalyst was found to be even higher than its solution counterpart under the same polymerization conditions. The addition of the filler in the polymer matrix led to an increase in composite rigidity as reflected by almost doubling the storage modulus at room temperature. Moreover, the filler affects the crystallization process, as observed by DSC and solid-state NMR, reducing the crystallinity up to 28% and the thickness of the rigid phase up to 22% compared with the neat sample.

1. Introduction

Polymer nanocomposites are a new class of composites of particle-filled polymers for which at least one dimension of the dispersed particles is in the nanometer range [1]. The incorporation of small amounts of exfoliated inorganic layered silicates with a high aspect ratio into a polymer matrix produces a material with mechanical properties, flammability, and barrier properties that are far superior to those of the base material. The high commercial importance of polyethylene (PE) has stimulated intense investigations of PE/layered silicate nanocomposites, and improvements of almost all the properties mentioned above have been reported in the literature [2–11].

There are three basic methods to prepare PE nanocomposites either in an intercalated morphology where silicate registry is retained or preferably in an exfoliated structure that is macroscopically isotropic. The first is to melt the intercalation of polyethylene into an organically modified silicate. With this method, the chemical modification of the layered silicates with alkylammonium ions containing long alkyl chain groups [5,7] or polymeric surfactants [6] has proven to be insufficient to form exfoliated nanocomposites, and generally a third component, e.g. polyolefin-*graft*-maleic anhydride, needs to be added as a compatibilizer in order to improve the dispersion of nanoscale clay pallets [5,8,9,11–13].

The second method is to form a nanocomposite by soaking the organo-silicates in a polyethylene solution. By removing the solvents the polyethylene is then intercalated into the silicate gallery. Based on this idea, a high-density polyethylene/organo-montmorillonite nanocomposite was prepared [14]. Intercalation was achieved but the presence of fairly large stacks indicated poor dispersion in this system.

The third strategy is *in situ* intercalative polymerization. With this technique, the catalyst for ethylene polymerization is introduced into the gallery of layered silicates, after which polyethylene forms *in situ* and the layer structure delaminates. This method has proved to be quite efficient in preparing exfoliated nanocomposites since the entropy resistance for the intercalation of polymer chains is significantly reduced and the heat released by polymerization acts favorably to reduce the process free energy. Actually, this *in situ* polymerization strategy has always been the popular way the Nylon/Montmorillonite (MMT) nanocomposites were prepared in the beginning [15]. Additional motivation to investigate this method comes from its potential application as a 'drop-in' process in the polyolefin industry, with no need to set up new equipment.

Considerable efforts were devoted to prepare polyethylene/layered silicate clay nanocomposites with different coordinated polyethylene catalysts and polymerization techniques. Typical Ziegler–Natta catalysts [16,17], metallocene catalysts [18–24], and late

* Corresponding author. Fax: +49 241 8022 185.
** Corresponding author. Fax: +86 571 87951227.
E-mail addresses: aadams@mc.rwth-aachen.de (A. Adams), wangjd@zju.edu.cn (J. Wang).

0032-3861/$ – see front matter © 2010 Elsevier Ltd. All rights reserved.
doi:10.1016/j.polymer.2010.08.037

transition metal Pd and Ni catalysts [25,26] were adopted to intercalate the silicate layer and initiate the ethylene polymerization. Exfoliated structures of nanoscale clay pellets could be obtained as observed from transmission electron microscopy (TEM) graphs and X-ray Diffraction (XRD) diffraction results. However, in order to locate the catalyst in the gallery of the layered silicates, functional groups needed to be introduced in the pallet surface of the silicate to react both with catalysts and co-catalysts [17,20,22]. An additional problem with this method was the dramatic loss of catalyst activity due to the chemically complex layer surface, especially in the case of metallocene catalysts, which in turn required the use of large amounts of expensive co-catalyst methylaluminoxane (MAO) [18–20,23,24].

Unlike the intercalation-exfoliation scheme and layered silicates, the nanocomposite precursor in the work reported in this contribution consisted of natural fibrous palygorskite clay. Palygorskite is a hydrated magnesium silicate with the theoretical half unit-cell formula $[(OH_2)_4(Mg,Al,Fe)_5(OH)_2Si_8O_{20}]\cdot 4H_2O$ [27,28]. A sketch of the palygorskite structure is provided in Fig. 1, from which the structural unit is shown to be a nanoscale fiber with several tens of nanometers in diameter and several hundreds of nanometers in length. The crystal lattice structure of palygorskite exhibits similarities to layered silicates in that the central octahedral sheet is sandwiched in between two tetrahedral silica sheets. However, it differs from common layered silicates in that, unlike layered silicates which lack a continuous octahedral structure, tetrahedral silica sheets are connected by inverted Si–O–Si bonds and are, therefore, continuous. This structural characteristic of the single nanofiber produces certain surface channels and internal tunnels, as shown in Fig. 1. Inside these channels and tunnels, zeolithic water is present under ambient conditions. The octahedral structure at the edge of the channels and tunnels is mainly comprised of a central magnesium cation coordinated by two water molecules. These coordinated water molecules, in turn, are hydrogen-bonded to zeolithic water in the nanopores of a single fiber.

By anchoring the catalyst on the surface of the single fiber and then initializing the polymerization of ethylene *in situ*, we showed that the produced polyethylene chain could encapsulate the fiber and lead to the exfoliated dispersion of nanoscale palygorskite into the polyethylene matrix. This special procedure to prepare exfoliated nanocomposites appeared to be more efficient because it avoided the pre-intercalation of polyolefin catalysts into galleries of layered silicates. This work demonstrates that the surface property of palygorskite after thermal treatment played a positive role in enhancing catalyst activity when a metallocene compound Cp_2TiCl_2 was loaded. The catalyst activity could be even higher than the corresponding solution catalyst, which was promising for the reduction of the co-catalyst dose.

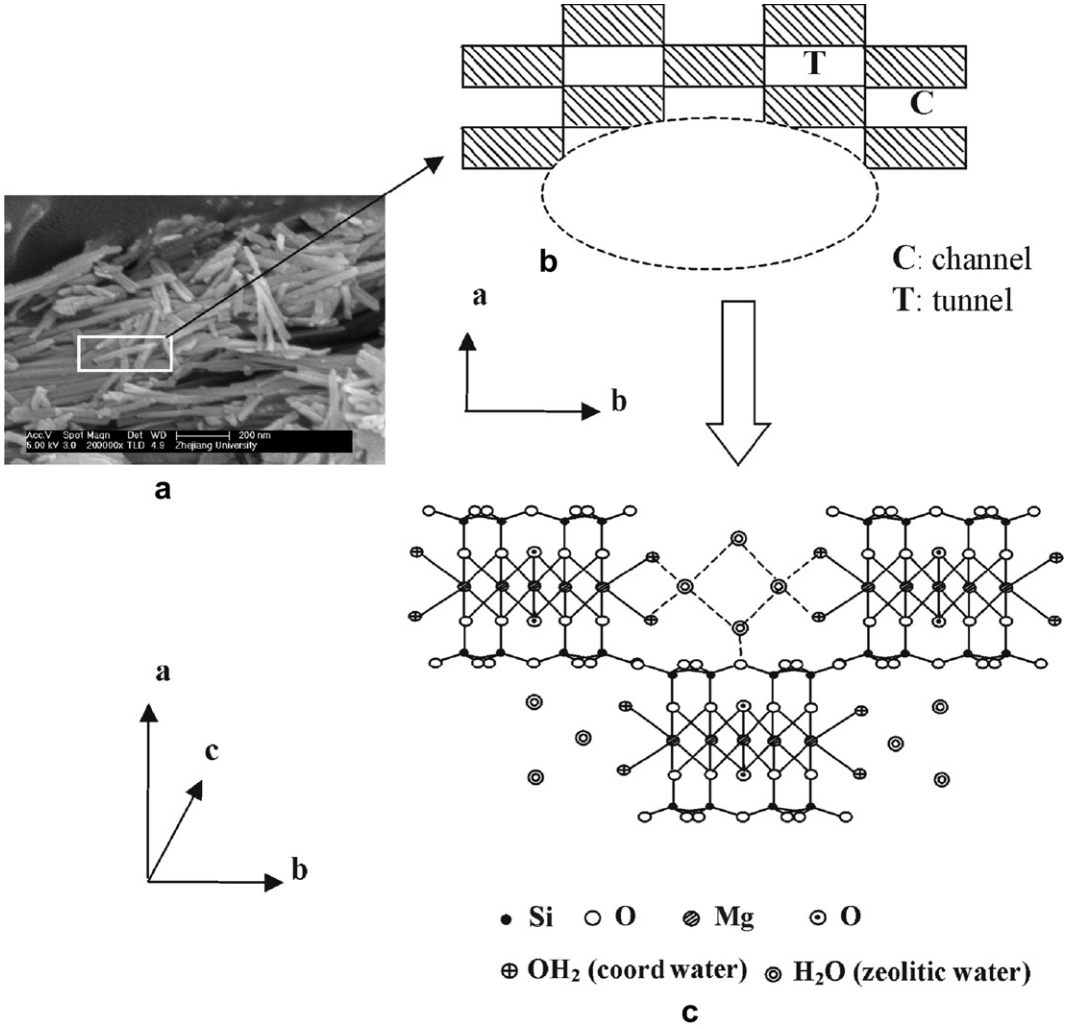

Fig. 1. Illustration of palygorskite microstructure: (a) SEM photograph of purified palygorskite sample with magnification times of 200,000. (b) Sketch of cross-section of single palygorskite fiber with pore structure occurring as channels and tunnels. (c) Lattice structure of palygorskite crystal and the expression of the different forms of water.

In the next step, the morphology and dynamic mechanical properties of the prepared nanocomposites have to be characterized. The molecular architecture of polymers in the solid state is of fundamental importance to understand the various macroscopic properties and to establish structure–property relationships. In this respect, all aspects related to the morphology including fraction composition, molecular mobility, and domain sizes have to be quantitatively determined and their correlation with the macroscopic properties have to be accurately known.

Solid-state NMR is one of the most informative techniques to characterize heterogeneous structures in polymers such as semicrystalline polyethylene [29–36]. Throughout the years, proton wideline NMR spectroscopy and relaxation experiments have frequently been applied to study the effect of chemical structure, molar mass, and thermal history on phase composition and molecular mobility in low and high-density polyethylene [31–35]. At temperatures well above glass temperature (T_g) of the amorphous phase, both the T_2-relaxation decay and wideline NMR spectra of PE can usually be decomposed into three components, which originate from a crystalline phase, a semi-rigid crystal–amorphous interface, and a soft fraction of the amorphous phase. The existence of a crystal–amorphous interface in semicrystalline polymers has been supported by both theoretical predication [37] and other independent experimental results obtained from procedures such as X-ray diffraction [38], transmission electron microscopy (TEM) [39], and comparisons between crystallinities, which were calculated according to Differential Scanning Calorimetry (DSC), Wide Angle X-ray Diffraction (WAXD), and density methods [40]. Moreover, ^{13}C NMR spectroscopy and relaxation experiments with different polyethylene samples have also explored a three-phase composition based on differentiating the chemical shifts of crystalline and amorphous phases [41–43]. Most recently, the effect of temperature and annealing on the domain sizes of high-density polyethylene has been studied by ^{1}H spin-diffusion NMR using a three-component structural model [44]. The obtained domain thicknesses are in good agreement with those measured by Small-Angle X-ray Scattering (SAXS) and transmission electron microscopy (TEM) on the same sample, indicating a good reliability of the spin-diffusion NMR method.

While the microscopic properties of various type of polyethylene were extensively investigated, the effect of fillers on the chain dynamics and structure in filled polyethylene as studied by solid-state NMR are rather limited [36,45]. By using a combination of proton and carbon experiments it was, for example, shown that when low-density polyethylene is filled with calcium carbonate, the filler reduces the mobility in the crystalline regions and affects the crystallization process [45].

In the present work, various ^{1}H solid-state NMR techniques, such as wideline spectra, longitudinal relaxation, and spin-diffusion measurements, were applied to characterize the effect that the palygorskite filler has on the morphology and chain mobility of the resultant, novel PE nanocomposites. On account of the very low content of paramagnetic Fe^{3+} ions in clay, the domain sizes of the different phases in the nanocomposites could also be estimated by spin-diffusion NMR. Here, a double-quantum filter was employed to select the magnetization from the rigid phase [46]. In this way, evidences about how the presence of the filler affects the crystallization behavior of the PE/nanocomposites and their morphology were obtained.

2. Experimental part

All manipulation of air sensitive compounds was carried out using standard Schlenk, vacuum, and glove box techniques. Argon or nitrogen was used as inert gas.

2.1. Materials

Bis–(cyclopentadienyl)titanium dichloride (Cp_2TiCl_2, ACROS Organics, USA) was purchased from J&K Chemical Corporation (Shanghai, China) and used as received. Toluene was dried over 4 Å molecular sieves for at least 10 days, then refluxed over sodium with benzophenone as an indicator and distilled under an argon atmosphere prior to use. Methylaluminoxane (MAO) in toluene (10 wt.%) was purchased from Albermarle Company (USA). Polymerization-grade ethylene was obtained from SINOPEC Shanghai Corporation (Shanghai, China) and purified by first passing it through M_n molecular sieves and then through 5 Å molecular sieves. Triisobutylaluminium (TIBA, Aldrich) in toluene (25 wt.%) was purchased from J&K Chemical Corporation. Palygorskite clay was kindly donated by AAC Company (Jiangsu, China) and purified according to the method described in the literature [47]. The particle size was selectively restricted to below 74 μm by passing the purified and ground palygorskite sample through a 200-mesh sieve. X-ray diffraction data and a mineralogical analysis [48] of the sample showed that the purity of palygorskite exceeded 95%, and impurities were trace amounts of quartz.

2.2. Preparation of palygorskite (PLT) supported catalysts

2.2.1. Cp_2TiCl_2/PLT

2.2 g of purified palygorskite was heated from room temperature to 500 °C with a rate of 5 K min^{-1} and kept at 500 ± 3 °C under nitrogen atmosphere for 4 h. The dried sample was then transferred to a Schlenk bottle and dried under a vacuum at 40 °C for an additional 2 h. The resulting solid was mixed with 0.20 mmol Cp_2TiCl_2 in 60 ml toluene and stirred for 24 h at 40 °C. After filtering the mixture, the obtained solid catalysts were washed six times with 50 ml of fresh toluene and dried under a vacuum at 40 °C for 3 h. The Ti content of the Cp_2TiCl_2/PLT supported catalyst was found to be 0.35 wt.% by using inductively coupled plasma-atomic emission spectroscopy (ICP-AES; IRIS Intrepid XSP; Thermo Elemental Corporation, USA).

2.2.2. Cp_2TiCl_2/PLT–MAO

2.2 g palygorskite was first dried as described above. Then, the dried palygorskite was mixed with 20 mmol MAO in 50 ml of toluene and afterwards the mixture was stirred for 6 h. The resulting solid was then washed three times with 30 ml of fresh toluene and dried under a vacuum at 40 °C to produce chemically modified palygorskite PLT–MAO. Then the impregnation of Cp_2TiCl_2 as described above was applied to PLT–MAO. The Ti content of the Cp_2TiCl_2/PLT–MAO supported catalyst was analyzed to be 0.70 wt.% by ICP-AES.

2.2.3. Cp_2TiCl_2/PLT–TIBA

2.2 g of purified palygorskite was heated to 150 °C under a nitrogen atmosphere with a rate of 5 K min^{-1} and kept at 150 ± 1 °C for 4 h. The solid sample was then transferred to a Schlenk bottle and dried under vacuum at 40 °C for an additional 2 h. Next, 20 mmol of Triisobutylaluminium (TIBA) in 30 ml toluene was added drop by drop to the clay/toluene slurry for 30 min. During this time an isothermal bath using ice water mixed with a prescribed amount of NaCl was used to maintain the reaction temperature of around −10 °C. After stirring for 24 h, the clay slurry was filtered and washed three times with 30 ml of toluene, and the obtained solid dried under a vacuum for 3 h at 40 °C to produce chemically modified palygorskite PLT–TIBA. The final impregnation of Cp_2TiCl_2 onto PLT–TIBA was the same as Cp_2TiCl_2/PLT–MAO. The Ti content of the Cp_2TiCl_2/PLT supported catalyst was found to be 0.49 wt.% by ICP-AES.

2.2.4. Cp_2TiCl_2/PLT–HCl

5 g of purified palygorskite was combined with 500 ml of HCl (1 M) at room temperature and stirred for 2 h at a rate of 350/min. After that, the solid part was separated using centrifugation and washed with distilled water until no residual Cl^- could be detected with $AgNO_3$. Then the sample was dried overnight at 60 °C to provide the palygorskite with HCl pretreatment. The resulting sample was ground and the part passing through a 200-mesh sieve was collected for the later supporting procedures. Both the thermal treatment process and the catalyst impregnation for PLT–HCl were the same as Cp_2TiCl_2/PLT. The Ti content of Cp_2TiCl_2/PLT–HCl supported catalyst was found to be 0.33 wt.% by ICP-AES.

2.3. Ethylene polymerization

Ethylene polymerization with a solution Cp_2TiCl_2 catalyst and supported catalysts were conducted in a 1 L stainless steel autoclave reactor equipped with a mechanical stirrer. The reaction temperature was regulated by a heating mantle and an internal cold water circuit. Before the start of polymerization, the reactor was set to 80 °C and purged five times with nitrogen and once with ethylene. Then the reactor temperature was set to 40 °C and 400 ml toluene was transferred to the reactor with a calculated amount of MAO co-catalysts. The ethylene pressure was fixed at 0.1 MPa for all experiments. Polymerization started by introducing solution or supported Cp_2TiCl_2 catalysts and continuously adding ethylene through a mass-flow meter (Brooks Instrument, 5850E series). Typically, after 1 h, polymerization was quenched by adding 20 ml of acidified ethanol, and the polymer was precipitated in 800 ml of ethanol, filtered and dried at 60 °C under a vacuum for 10 h.

2.4. Preparation of compression-molded specimen for mechanical testing

Powder samples of neat polyethylene and polyethylene/clay nanocomposites were first heated to 170 °C for 3 min and then molded at 180 °C for 10 min at 10 MPa. The molded sheets were cooled down to ambient temperature at the same pressure. Samples with dimensions of $15 \times 10 \times 1.5\ mm^3$ were cut from the molded sheets for dynamic mechanical analysis.

2.5. Characterization of palygorskite

The morphology of purified palygorskite was investigated using FSM SIRION-100 (FEI Corp., USA). The sample was sputter-coated with gold before observation. A thermogravimetric analysis was carried out on a TGA/SDTA851^e instrument (METTLER Corp., Switzerland). The N_2 flow rate was fixed at 20 ml min^{-1}. Heating took place from 30 °C to 1000 °C at a rate of 10 K min^{-1}. X-ray diffraction spectra of clay samples were recorded on a Rigaku D/Max-RA diffractometer (Japan) with Cu Kα radiation (40 kV, 80 mA). Scanning was done in 0.02° steps at a speed of $2^\circ \cdot min^{-1}$.

2.6. Characterization of neat PE and PE/palygorskite nanocomposites

Differential Scanning Calorimetry (DSC) measurements of polyethylene and PE/clay nanocomposites were performed on a DSC-7 instrument (Perkin–Elmer Corp., USA). Samples (of about 5 mg each) were first heated to 180 °C at a rate of 10 K min^{-1} and then cooled down to 50 °C at the same rate. The second heating cycle was used to acquire the DSC thermograms, also at a heating rate of 10 K min^{-1}. The average molecular weight and molecular weight distribution were determined using gel permeation chromatography (GPC) at 150 °C on a PL-GPC-220 instrument with

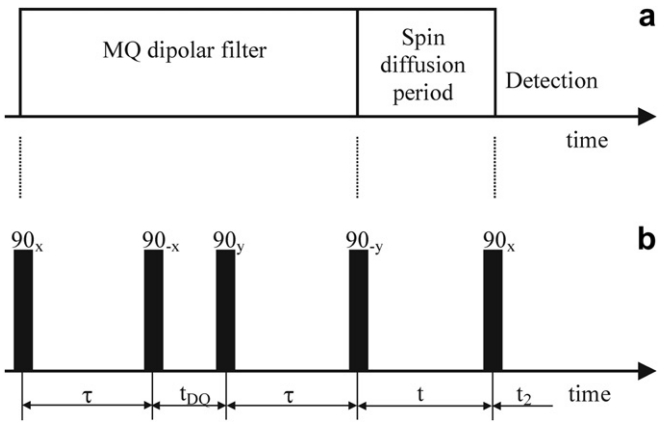

Fig. 2. (a) General scheme of a spin-diffusion NMR experiment using a multiple-quantum (MQ) dipolar filter. (b) Pulse sequence used for the spin-diffusion NMR experiment with a double-quantum filter.

1,2,5-trichlorobenzene as a solvent. A dynamic mechanical analysis (DMA) was carried out with a TA Q800 (USA) at fixed frequency (1 Hz) with a heating rate of 3 K min^{-1} between −135 °C and 145 °C. Transmission electron micrographs were obtained with a Phillips CM100 apparatus using an acceleration voltage of 100 kV. The samples were 80 nm-thick and prepared with an ultra cryomicrotome cutting at −130 °C.

2.7. Solid-state 1H NMR measurements

Proton solid-state NMR spectra, longitudinal magnetization relaxation (T_1), double-quantum (DQ) build-up curves, and spin-diffusion data were measured on a Bruker DSX-500 spectrometer working at a proton frequency of 500.12 MHz. The data were collected at room temperature for non-spinning samples. The duration of the 90° pulse was 2.5 μs and a recycle delay of 5 s was used for all experiments.

The experimental wideline spectra were separated into three components using the DMFIT software [49]. The broad component of the spectra was approximated by a Gaussian function while that of the mobile amorphous component was estimated by a Lorentzian line shape. For the intermediate phase a combination of the two functions was used [44]. In order to simplify the fitting procedure due to the high amount of parameters involved, the positions and the line widths of the three components were set to the values obtained from the DQ filtering experiments.

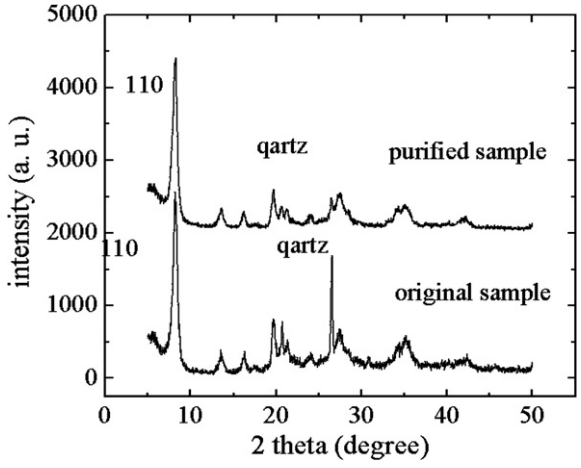

Fig. 3. X-ray diffraction spectra of crude and purified palygorskite.

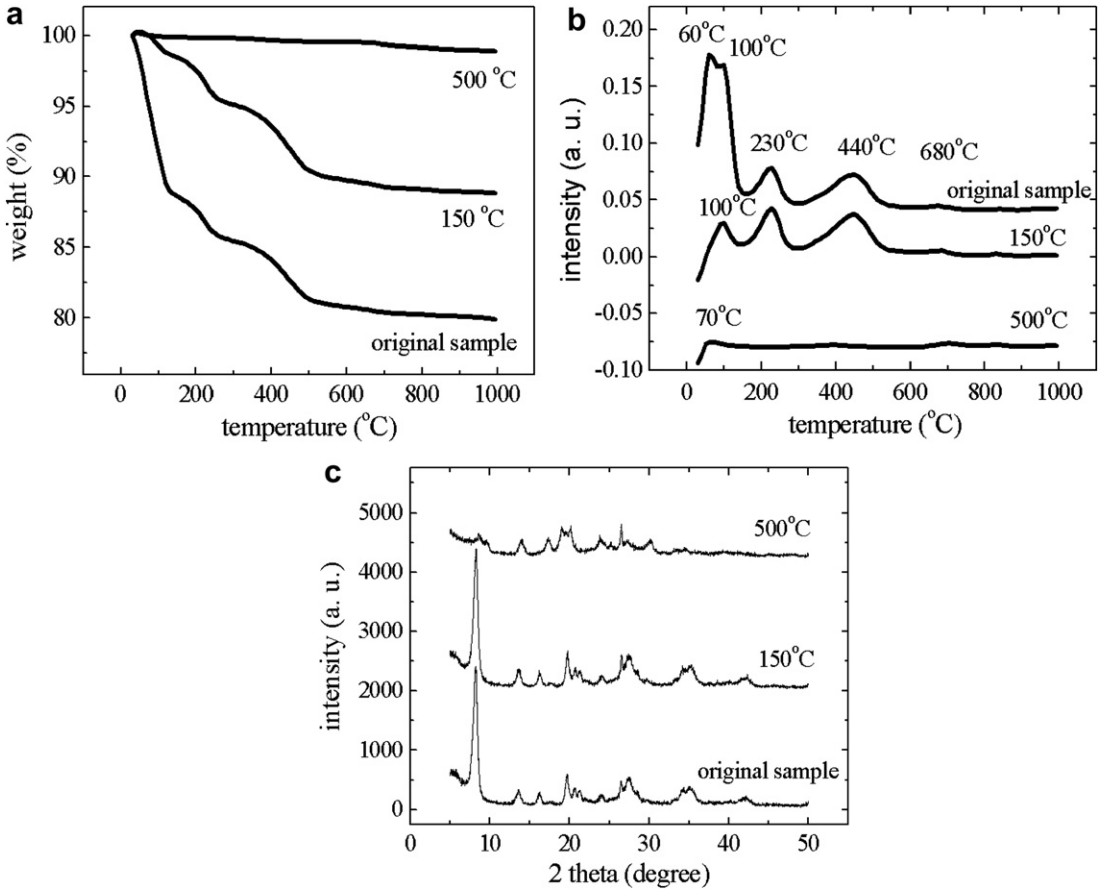

Fig. 4. (a) TG traces of palygorskite at ambient temperature, thermally treated at 150 °C and at 500 °C. (b) Differential TG curves extracted from (a). (c) X-ray diffraction spectra of palygorskite at ambient temperature, and thermally treated at 150 °C and at 500 °C. In the figures (b) and (c) the three curves are shifted along the *y*-axis for a better understanding.

Proton longitudinal magnetization relaxation (T_1) experiments were performed using inversion-recovery method. Typically 35–40 time increments were used and the growth of the total integral intensities of the NMR absorption spectra were evaluated with a least-squares fit using a sum of two exponential functions.

Proton spin-diffusion measurements were performed using the general scheme consisting of a *z* magnetization filter, a spin-diffusion period, and an acquisition period as presented in Fig. 2a.

Table 1
Ethylene polymerization with solution and palygorskite supported Cp_2TiCl_2 catalysts.

Catalyst[a]	Ti load[b]	Cat. Conc. In [μmol/L][c]	Al/Ti mole ratio	Catalyst activity[d]
Cp_2TiCl_2	–	10	2000	1062
Cp_2TiCl_2/PLT	0.35%	10	2000	1151
Cp_2TiCl_2/PLT–MAO	0.70%	10	2000	260
Cp_2TiCl_2/PLT–TIBA	0.49%	10	2000	388
Cp_2TiCl_2/PLT–HCl	0.33%	10	2000	–
Cp_2TiCl_2/PLT	0.35%	50	300	587

The amount of supported catalyst in each run was determined by the prescribed molar concentration of Cp_2TiCl_2 and the Ti load of the supported catalyst. For each run, the catalyst amount is 3 μmol.

[a] PLT: palygorskite, PLT-MAO: playgorskite with chemical treatment of methyl-aluminoxane (MAO), PLT–TIBA: playgorskite treated with triisobutylaluminium (TIBA), PLT-HCl: palygorskite pretreated with dilute HCl.

[b] Loaded amounts of Ti are in gram of metal per gram of supported catalyst (including catalyst and the support).

[c] The catalyst concentration in the polymerization vessel was calculated based on the moles of Ti.

[d] Catalyst activities are in kg PE produced by per-mol Ti per hour and were calculated from the mass of the polymer, the catalyst concentration, and the polymerization time.

Several recent publications demonstrated that the use of a filter based on the excitation of double-quantum (DQ) coherences represent one of the best choices compared to filters that select the mobile phase [44,46,50,51]. This is mainly due to a more accurate detection of the narrow signals on top of the broad component compared to the detection of a broad component under a narrow signal, as is the case of "mobile" filters. This present study used the dipolar filter based on the pulse sequence depicted in Fig. 2b. As the spin-diffusion takes place on a time scale comparable with the

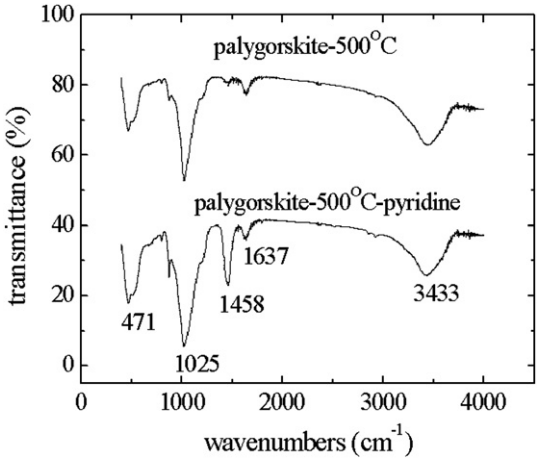

Fig. 5. FTIR spectra of the thermally treated palygorskite before and after pyridine adsorption.

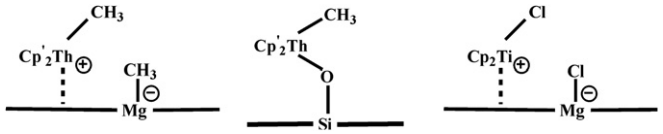

Fig. 6. Surface species model for metallocene compounds adsorbed on inorganic supports.

longitudinal relaxation time of the amorphous component a correction of the T_1 effects has been implemented.

3. Results and discussions

3.1. Surface property of palygorskite

Fig. 3 compares the XRD spectra of industrial and purified palygorskite. In quartz, the diffraction peaks are found to be greatly reduced by purification while the diffraction peaks in crystal palygorskite do not observably change. As already mentioned in the introduction, there are basically three kinds of water molecules that can be differentiated inside the palygorskite sample before it is thermally treated: surface bound water, zeolithic water, and coordinated water. All of them are clearly denoted in Fig. 1. These water molecules are further revealed in the TG analysis curves shown in Fig. 4a and b. Original palygorskite shows five weight-loss peaks in the DTG curve: peaks at 60 °C and 100 °C, which correspond to surface water and zeolitic water, respectively; peaks at 230 °C and 440 °C, which correspond to the first and second coordinated water, and a peak at 680 °C, which corresponds to structural hydroxyl water [27,28].

On account of these characteristics of the palygorskite structure, it is essential to remove all water in a controlled manner since, on one hand, water is poisonous to the cationic active centre and, on the other hand, water found in the crystal structure of some inorganic salts can be used to react with alkyl aluminium. In this case aluminoxane is generated, which is known to react towards metallocene compounds by anchoring them through ionic bonds [52]. Different treating temperatures were selected to remove surface adsorption water zeolitic, water and, additionally, coordinated water. Once the coordinated water was removed, the pore structure collapsed and the 110 diffraction peak in the XRD spectrum gradually disappeared [28]. Palygorskite after thermal treatment at 150 °C and 500 °C was analyzed using TG and XRD. The results presented in Fig. 4 indicate that at low temperature, thermal treatment removed both the surface water and zeolitic water, while the crystal structure of palygorskite remained unchanged. At higher temperature, however, thermal treatment removed all water except structural hydroxyl, and the 110 diffraction peak almost disappeared. The small peaks that could be seen in the DTG curves at 100 °C for PLT-150 °C and 70 °C for PLT-500 °C were attributed to air contact that occurred during the TG analysis, a phenomenon that could hardly be avoided in the present stage.

3.2. Polymerization with palygorskite supported Cp_2TiCl_2 catalysts

The results of ethylene slurry polymerization with different supported catalysts are listed in Table 1. The solution polymerization with Cp_2TiCl_2 under the same conditions was also performed for comparison. It is well known that the supporting of metallocene compounds on inorganic carriers such as silica or clay mineral significantly reduces the catalyst activity because of the complex chemical environment and the strict hindrance of the support surface [19,20,53]. In this respect, a chemical modification of the carrier surface with alkyl aluminium or alkyl aluminoxane was necessary to enhance catalytic activity [53].

Compared to other supported catalysts with the chemical modifications of palygorskite the Cp_2TiCl_2–PLT catalyst produced the highest activity, comparable to that of a solution polymerization with equal amounts of Ti, as shown in Table 1. This observation is most likely explained by the surface property of the supporting materials since they supplied a different chemical environment for the final cationic active center. Interestingly, we found that some supported Cp_2ZrCl_2 catalysts on calcined H-ZSM-5 [54] and Al-MCM41 [55] displayed a polymerization behavior that was similar to the PLT–Cp_2TiCl_2 system. All the inorganic carriers were characterized by strong surface Lewis acidity, and as previously mentioned, the surface Lewis acidity played an important role in enhancing the catalyst activity.

Therefore, the surface property of palygorskite was investigated by the pyridine adsorption experiment. First, the clay was thermally treated at 500 °C and then exposed to a continuous pyridine flow. This flow was carried by nitrogen for a certain time and then measured with FTIR [56]. The results are displayed in Fig. 5. A strong adsorption peak at 1458 cm^{-1} was found with the pyridine adsorbed palygorskite, which was attributed to the adsorption of pyridine on Lewis acid sites (1447–1460 cm^{-1}). Pyridine chemisorbs on Brønsted sites known as pyridinium ions, which give rise to bands at 1530–1540 cm^{-1} [56,57]. These were absent in the IR spectra of PLT-500 °C, indicating that the surface of PLT-500 °C was mainly occupied by Lewis acid sites. This conclusion was consistent with the results from FTIR analyses of the surface property of sepiolite, the homologue clay mineral of palygorskite [58].

According to the literature [27,28], the generation of Lewis acid sites on the palygorskite surface, is attributed to the loss of water molecules combined with a build-up of magnesium in the edge lattices, which is why a large amount of coordinatively unsaturated magnesium occurred. Based on this result, we treated palygorskite with dilute HCl, a method that has been commonly used to remove metal cations in edge lattices [27]. Both the thermal treatment used and the supporting process of the magnesium-washed palygorskite were exactly the same as PLT-500 °C. Nevertheless, the resulting supported catalyst generated a certain amount of trace activity for ethylene polymerization. This experimental outcome further illustrated that, after thermal treatment, the Lewis acidic property of palygorskite was associated with a high catalytic activity of theCp_2TiCl_2/PLT supported catalyst.

Table 2
Ethylene polymerization using solution and palygorskite supported Cp_2TiCl_2 catalysts activated by MAO.

Sample	Polymerization time [min]	Catalyst activity[a]	Amount (g)	Filler load[b]	M_w	M_w/M_n	T_m [°C]		ΔH_m [J/g]	
							First scan	Second scan	First scan	Second scan
PE	25	469	9.7	–	19,1056	3.2	135.3	136.2	205	180
NC1	100	324	27.0	2.3%	31,4807	3.4	137.2	134.7	216	153
NC2	50	366	15.3	4.1%	21,0371	3.3	137.1	134.8	207	149
NC3	25	499	10.4	8.1%	31,9017	2.8	136.4	134.8	163	119

[a] Catalyst activity is recorded in kg·(mol of Ti)$^{-1}$ h^{-1}.
[b] The load of palygorskite was determined by TG analysis with the heating temperature ranging from 30 °C to 700 °C and a heating rate of 10 K min^{-1}.

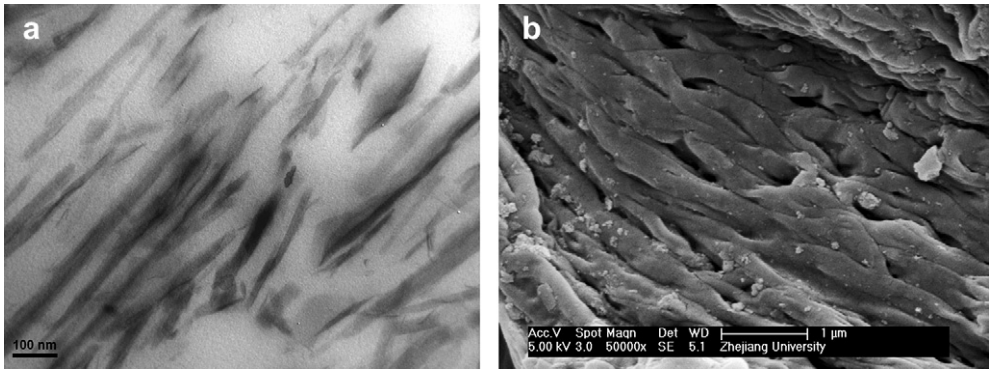

Fig. 7. (a) TEM and (b) SEM photographs of the NC3 sample with the magnification factors of 150,000 for (a) and 50,000 for (b).

Although the strength of the surface Lewis property of palygorskite was revealed by the pyridine adsorption experiment, the precise form of the anchored active species was not well known at this stage. According to the *in situ* CPMAS NMR study of $Cp_2'Th(^{13}CH_3)_2$ adsorbed in various inorganic supports for the polymerization of ethylene [59], the adsorbate structure could have been very different based on the surface acidity of the supports. In the case of Lewis acidic supports, such as dehydroxylated Al_2O_3 and $MgCl_2$, a "Al–CH_3" or "Mg–CH_3" ^{13}C resonance was observed and accompanied by residual low field Th-$^{13}C(\alpha)H_2R$ adsorbate resonances.

As a result, a "cation-like" species, which was displayed in Fig. 6a [57] and formed by the transfer of alkyl groups to acceptor sites on the surface may have been highly active in ethylene polymerization. In partially dehydroxylated silica, however, an extensive Th–CH_3 protonolysis occurred, and the CPMAS spectroscopy indicated that the Th-$^{13}C(\alpha)H_2R$ resonance was at a considerably higher field, without any evidence of a transferred surface alkyl group. Thus a "μ-oxo-like" structure, displayed in Fig. 6b, was suggested for the adsorbate [57] and showed low activity or trace activity for ethylene polymerization. Although we had no experimental evidence at this point, we believed that a transfer of ancillary ligand from the Cp_2TiCl_2 to the acceptor sites on the palygorskite surface had taken place and that a "cation-like" adsorbate structure had formed during the supporting process, as displayed in Fig. 6c. This "cation-like" species was responsible for the high activity of the directly supported catalyst. A chemical treatment of the support might have covered the surface Lewis sites, and active species with the general form in conventional supported metallocene catalyst systems occupied and reduced catalytic activity during the ethylene polymerization.

3.3. Preparation of polyethylene/palygorskite nanocomposites

The directly supported catalyst Cp_2TiCl_2/PLT was selected to prepare polyethylene/palygorskite nanocomposites because of its high catalyst activity. The reduction of process complexity was a further consideration, since it required no chemical modification of the clay material. A simple way to control filler loading inside the polyethylene matrix was to adjust the polymerization time while keeping the other parameters unchanged. The results of the polymerization and polymer characterizations are listed in Table 2.

The polymerization results listed in Table 2 show that the activity of the supported catalyst, once again, was comparable to the homogeneous catalyst under the same polymerization conditions when the concentration of the catalyst was increased. Consistent with the general results obtained from the ethylene polymerization of supported metallocene catalysts, the molecular weights of polyethylene increased when the supported catalyst was used [53].

3.4. Characterisation of the nanocomposites by electron microscopy and DSC

The nascent nanocomposite (NC) powder sample was observed by Scanning Electron Microscopy (SEM), and the molded one was examined by TEM (Fig. 7). As evident from the TEM photograph, palygorksite was dispersed mainly in the form of a single fiber inside the polyethylene matrix. Interestingly, we also observed the polyethylene 'noodle' structure in the SEM photograph of the nascent nanocomposite powder sample, as shown in Fig. 7b. Based on the theory of 'morphology replication' for polyethylene catalysts

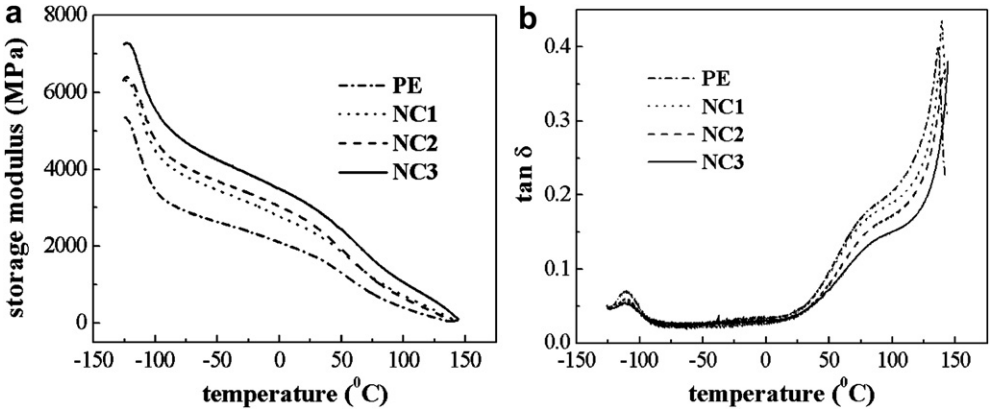

Fig. 8. Temperature dependence of (a) storage modulus and (b) tanδ for PE and PE/palygorskite.

Table 3
Dynamic storage moduli of PE and PE/palygorskite nanocomposites at different temperatures.

Sample	Storage moduli [GPa]		
	−80 °C	−30 °C	30 °C
PE	2.97	2.45	1.71
NC1	3.89	3.20	2.32
NC2	4.13	3.44	2.49
NC3	4.82	3.95	2.94

supported by silica [60], we believed that this polyethylene 'noodle' morphology might be a replication of the fiber structure of palygorskite. However, the diameter of a single polyethylene noodle was estimated to be around several hundreds of nanometers, so that in one PE noodle there might have been several individual palygorskite fibers.

In addition, some of the PE noodles were found to be composed of several smaller ones. These observations presented a view of the *in situ* polymerization process using the Cp_2TiCl_2/PLT supported catalyst: PE chains grow from the active sites anchored on the surface of palygorskite fiber and then encapsulate the single fiber to form the basic units of the PE 'noodle' structure. Because polyethylene chains are so entangled, it was possible to connect adjacent units to achieve a morphological replication of both single fibers and fiber clusters.

For the DSC experiments first and second thermograms were recorded using the same heating rate. In the case of neat PE samples, the melting point in the second scan slightly increased while enthalpy decreased. The cause might have been an increase in the thickness of the lamellae due to a rearrangement of PE chains in the bulk state and the melting of small crystallites. In the case of NC samples, however, the melting points and the melting enthalpy always decreased in the second scan. The increase in filler loading led to a further decrease in the melting enthalpy while no obvious impact could be seen on the melting points.

This observation clearly showed the effect of nanoscale fillers on the crystallization of PE, especially from the bulk state. If the heat of a fusion (ΔH_m) of 100% crystal-core polyethylene was taken as 293 J/g [61], then the crystallinity of PE decreased from 61% to 41% (results from the second scan) when filler loading was increased from 0% to 8.1%. This dramatic decrease in PE crystallinity with up to 28% with an increase in filler loading was also observed with PE/layered silicates nanocomposites prepared by *in situ* polymerization [17,20].

3.5. Dynamic mechanical analysis of the NC samples

Plots of the storage modulus and tanδ against temperature were recorded and are shown in Fig. 8a and b, respectively. Overall, the storage modulus of pure PE was found to be lower than that of NC samples. When the filler loading was 2.3% (NC3), an obvious increase of storage moduli had occurred. A further increase in filler loading to 4.1% (NC2) did not lead to a remarkable enhancement of the modulus. Finally, when the filler loading reached the highest value, a notable increase in the modulus was again observed. Selected storage modulus values of PE and PE nanocomposites at different temperatures in the plateau area of the DMA curves are listed in Table 3.

The large increase in moduli is a common characteristic feature of layered silicate-based nanocomposites in which a small amount of inorganic filler is enough to remarkably improve the mechanical properties [1]. The results presented in this work thus illustrate that palygorskite may be an alternative choice. The enhancement of the storage modulus represented over 30% (−30 °C) with 2.3% of filler loading and could have further reached 60% with 8.1% of filler contents. The improvement in the storage modulus was comparable to some layered silicate filled polyethylene prepared by both *in situ* polymerization [20] and melt compounding [11]. However, it should be noted that the significant decrease in PE crystallinity in the NC samples, as reflected in the DSC results, may have counteracted this reinforcement effect to some extent. This deduction is supported by the comparison between the modulus curves of NC2 and NC3, where a filler of nearly double the size only led to a slight increase in the storage modulus. As a result, the final mechanical property of nanocomposites was determined by the interplay of the decrease in PE crystallinity and the reinforcement of the filler.

Based on the dependence of tanδ on the temperature of pure PE and PE/clay nanocomposites, two transitions were observed for all samples at ca. −110 °C and 70 °C consistent with the typical DMA curves of highly linear HDPE which, in turn, were characterized by a weak transition at ca. −20 °C [62]. The transitions at ca.−110 °C, −20 °C, and 70 °C are denoted by γ, β, and α, respectively. The γ relaxation is commonly ascribed to the glass transition and therefore concerns the amorphous fraction of the polymer matrix [63,64]. The β transition is related to the glass–rubber transition of constrained non-crystalline chain segments [63,64]. Here, we found out that the β transition was more prominent in branched polyethylene samples whereas it could hardly be observed in linear HDPE. The mechanism for the

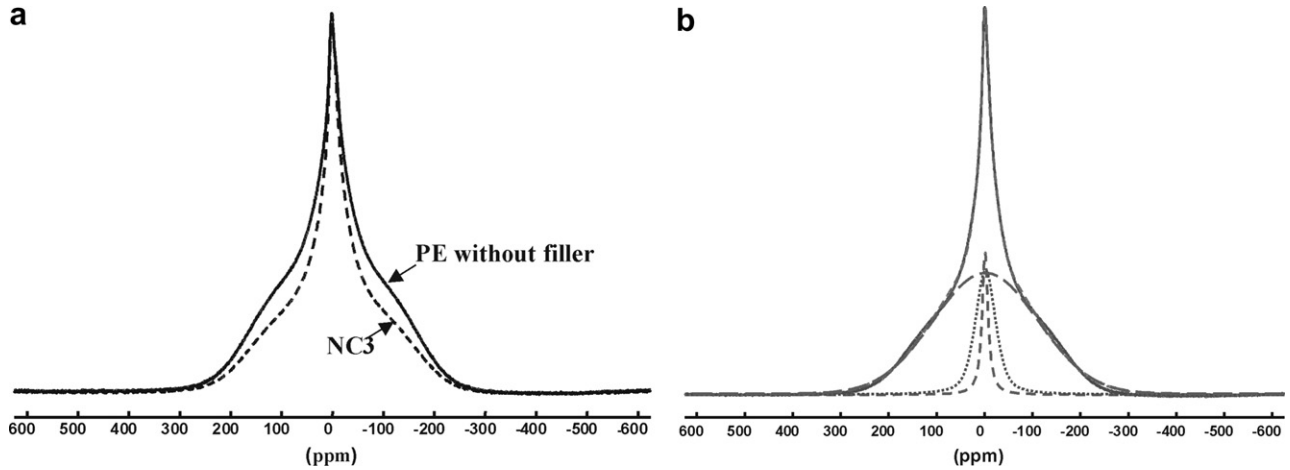

Fig. 9. (a) ^{1}H NMR spectra of neat PE and PE/palygorskite nanocomposite (NC3) and (b) a typical decomposition of the spectrum of NC3 revealing the signals of the three different fractions: rigid fraction (broad Gaussian line), interface (intermediate line shape), and mobile amorphous fraction (narrow Lorentzian line).

Table 4
Phase composition and line widths at half height for the neat and palygorskite filled polyethylene.

Sample	DSC crystallinity [%]	Rigid phase [%]	Interface [%]	Amorphous phase [%]	$\Delta\nu_{1/2}$ Rigid [kHz]	$\Delta\nu_{1/2}$ Interface [kHz]	$\Delta\nu_{1/2}$ Amorphous [kHz]
PE	65.1	79.2	15.6	5.2	52.9	10.72	4.88
NC1	57.5	72.4	18.9	8.7	51.9	10.82	4.96
NC2	56.4	70.6	19.6	9.8	51.3	11.94	5.07
NC3	46.4	66.3	22.4	11.3	51.0	13.84	7.58

β transition correlates with the relaxation of branching points in polyethylene [65]. The α relaxation process is associated with phenomena such as intracrystalline relaxation and the sliding of chains tied within crystalline blocks [66]. The results shown in Fig. 8b illustrate that both the amorphous and crystalline parts of PE were affected by the introduction of the nanoscale filler. When filler loading increased, the α transition peak significantly decreased, an occurrence that could have been related to the decline in PE crystallinity as characterized by DSC for bulk crystallized samples. In addition, we found that γ transition peaks were generally weaker when the filler was introduced and that their intensity further declined as filler loading increased. This observation may indicate a constraint of the molecular motions in the amorphous part.

3.6. Solid-state NMR experiments

3.6.1. Phase composition and chain mobility

As depicted in Fig. 9, differences can be seen between the NMR signals of the sample with a filler content of 8.1 wt.% and that without. In order to quantify the changes induced by the filler, a decomposition of the spectra has to be done. The best fit of our data could be obtained by using a combination of three components corresponding to the rigid phase (often called NMR crystallinity), interface, and mobile amorphous phases for the neat PE as well as for the nanocomposites. The fractions and half-height line widths corresponding to the various phases of the investigated samples are summarized in Table 4 together with the corresponding DSC crystallinity for the purpose of comparison.

The obtained results indicate that the presence of the filler in the matrix is affecting both the phase composition and the chain dynamics. A decrease of the rigid phase is observed with increased amount of filler. The same trend is detected by DSC only that the amount of the DSC crystallinity is lower than the amount of the rigid phase as seen by NMR. The differences observed between the two methods are related to the fact that at room temperature the NMR rigid phase is including not only the crystalline phase but also a part of the interface existing between the rigid phase and the mobile amorphous phase. Differences between DSC and NMR data at room temperature, in the same range with our results, are reported, for example, by Cheng for samples very close with our neat PE sample [41]. They report a DSC crystallinity of about 64% and an NMR crystallinity of about 82% [41].

The observed decrease in the rigid phase/crystallinity in the case of our nanocomposites compared with the neat sample and with increasing filler load can be related to the effect that the filler has on the crystallization process. The presence of the filler during the preparation of the nanocomposites leads to difficulties for the polymer chains to arrange themselves in a similar manner as in the neat polymer which will have as direct consequence a decrease of the crystallinity [17,20]. On the other side, we can also detect a small effect of the filler on the chain dynamics of the rigid phase. A slight decrease in the line width is observed between the neat sample and the nanocomposites. However, for a better evidence of the immobilization of the chains in this phase more sensitive NMR measurements are required and work along this line is in progress.

Beside the estimation of the amount of the rigid phase, NMR provides information about the effect of the filler on the other phases. We observe that the amounts of the interface and mobile amorphous phase are increasing with increasing the amount of filler from 0% to 8.1%. Moreover, the chain dynamics in both phases become more restricted compared with the neat sample and with increasing the amount of filler.

Table 5
Proton longitudinal relaxation times of neat PE and PE/palygorskite nanocomposites.

Sample	T_1^{long} [ms]	T_1^{short} [ms]	A^{long} [%]	A^{short} [%]
PE	1770	412	96.50	3.50
NC1	1580	433	94.40	7.60
NC2	1560	442	91.71	8.29
NC3	1560	458	90.95	9.95

3.6.2. Proton longitudinal relaxation times

Naturally occurring palygorskite contains Fe^{3+} ions with a content of 3.9 (wt.%) as determined by elemental analysis. These ions are mainly placed in inner octahedral positions [27,28] and in these distorted environment they are strongly paramagnetic. These paramagnetic impurities can have a big influence on the spin-lattice relaxation time of the protons in their proximity and consequently of the protons further away by spin-diffusion. As very nice shown by VanderHart in nanocomposites of nylon 6 with montmorillonite, the above described effect can be used to estimate the quality of the clay dispersion [68,69]. In the case of good exfoliation the effect of the Fe^{3+} on the T_1 is the strongest. Additionally, the presence of an effective paramagnetic ion will also lead to a broadening of the line width which can influence the study of the real chain dynamics. Therefore, the effect of paramagnetic Fe^{3+} ions on the proton longitudinal relaxation time has to be critically examined in order to get information about the right interpretation of our wideline data and about the extent to which spin-diffusion

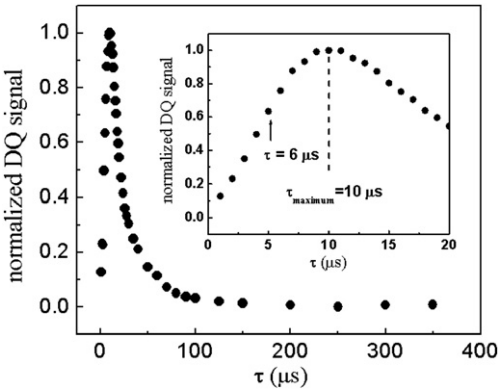

Fig. 10. Proton double-quantum (DQ) NMR build-up curves for the NC3. In the insert, the initial part of the DQ build-up curve is shown. The arrow corresponds to the excitation/reconversion time $\tau = 6$ μs used for the DQ filter.

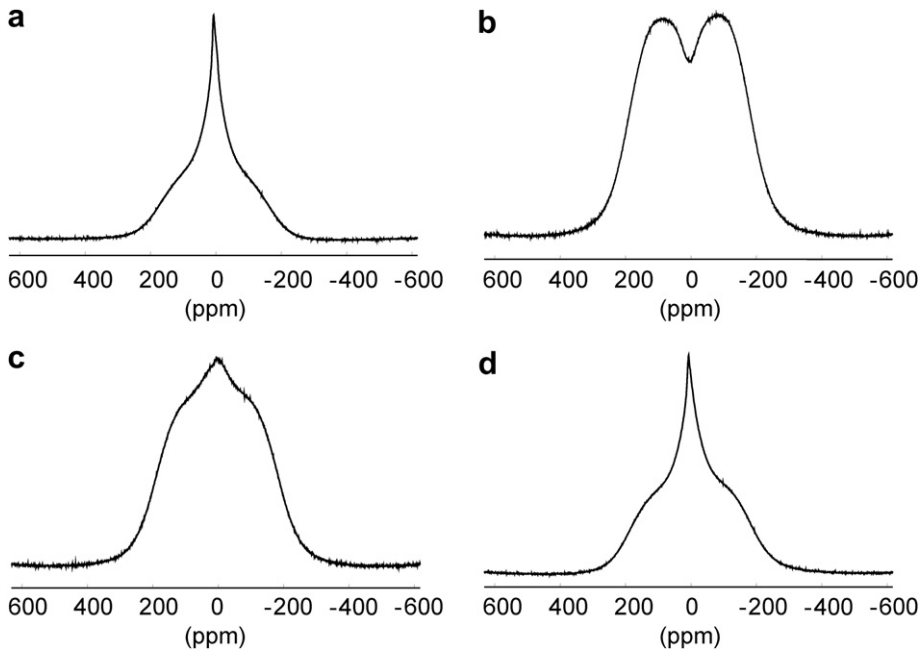

Fig. 11. (a) ^{1}H NMR spectrum of NC3. (b) ^{1}H double-quantum NMR filtered signal of the rigid phase. (c) Evolution of the magnetization after a diffusion time of 100 μs. Signal from the interface appears. (d) Evolution of the magnetization after a diffusion time of 150 ms. The signal now contains contributions from all phases and approaches the equilibrium signal. The spectra are normalized to the same intensity for a better view.

experiments could be performed on our systems. The recovery of the magnetization could be well fitted with a sum of two components indicating that the spin-diffusion process is only effective between the rigid phase and the interface. By comparing the obtained results, which are summarized in Table 5, with those from wideline we can conclude that the long component is attributed to the rigid phase and to the interface while the short component belongs to the amorphous phase. The values estimated for the amounts of the two phases for the different amounts of filler are mainly the same like those obtained from the wideline data.

By comparing the values obtained for the nanocomposites with those obtained for the neat sample, it is clear that the morphology of the nanocomposites is affected by the introduction of the filler. The long component of the measured T_1 values for the nanocomposites is lower than that of the neat sample but the effect is relatively small. For exfoliated samples containing almost the same amount of filler and paramagnetic ions the T_1 value decreased to about half of the value obtained for the neat sample. Moreover, no changes can be observed with increasing the amount of the filler.

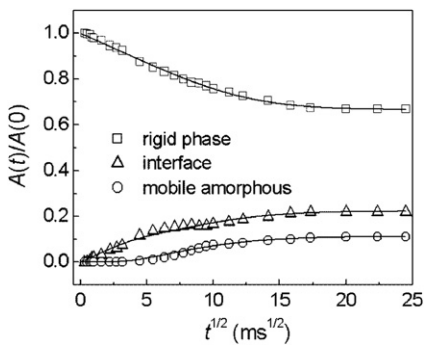

Fig. 12. Typical spin-diffusion curves of filled polyethylene. The lines represent the theoretical spin-diffusion curves obtained in the approximation of a lamellar morphology.

For the amorphous component higher values of the relaxation times are observed in the nanocomposites than in the neat sample. Additionally, with increasing the amount of the filler an increase is seen which indicate that the presence of the filler leads to an immobilization of the chains in this phase. This effect is in agreement with the findings from the broadline data. Therefore, the case of our samples the reduction in the relaxation times of the rigid phase/interface cannot be attributed to the presence of effective Fe^{3+} ions. The Fe^{3+} ions are located to such a distance from the protons close to the clay that they are not efficient in reducing their T_1. From the TEM data it is clear that the nanocomposites exhibits an exfoliated structure but, based on the NMR data, however, it is difficult to obtain information about the quality of the clay dispersion [69]. Nevertheless, we can conclude that the Fe^{3+} ions present in the clay do not affect the spin-diffusion experiments.

3.6.3. Double-quantum dipolar filter

The dipolar filter based on the excitation of double-quantum coherences edits different dipolar spin networks as a function of the excitation/reconversion time τ. Using this property, different phases in polyethylene and its nanocomposites can be selected by a proper choice of excitation/reconversion time. The enhanced chain motions in the interface and amorphous fraction reduce the strength of proton dipole–dipole interaction compared to that in the rigid phase. Therefore, the DQ filter could be set to select only the magnetization from the most rigid fraction where the strongest dipolar couplings exist. In this case, the magnetization from the interface and mobile amorphous fraction is filtered out due to weaker dipolar couplings. In order to determine the optimum τ value of the DQ filter, DQ build-up curves were recorded for all samples. A typical DQ build-up curve for the nanocomposites is shown in Fig. 10. The maxima of the DQ build-up curves appeared at very short excitation/reconversion times τ of approximately 10 μs for all samples. By choosing $\tau = 6$ μs, the mobile component and the interface were completely filtered out as shown in Fig. 11, and this selection still kept the signal-to-noise ratio at a reasonable value.

Table 6
Spin-diffusion coefficients (D) and domain sizes (d) of rigid, interface, and mobile amorphous phases for neat PE and PE/palygorskite nanocomposites.

Sample	D_{rigid} [nm^2/ms]	d_{rigid} [nm]	$D_{interface}$ [nm^2/ms]	$d_{interface}$ [nm]	$D_{amorphous}$ [nm^2/ms]	$d_{amorphous}$ [nm]	L [nm]
Neat PE	0.320	27.6	0.199	2.7	0.079	1.8	34.8
NC1	0.313	24.6	0.196	3.2	0.080	2.9	33.9
NC2	0.310	23.1	0.195	3.4	0.081	3.2	33.1
NC3	0.308	21.6	0.203	3.6	0.099	3.7	32.5

3.6.4. Thickness of domains by 1H spin-diffusion

The proton spectra acquired after different spin-diffusion times t are shown in Fig. 11. From these spectra, the flow of longitudinal magnetization from the rigid fraction to the interface and then to the mobile amorphous fraction can clearly be identified. The time-dependent integral spin-diffusion intensities of the three components obtained for the NC3 sample are plotted in Fig. 12. Generally, the quasi-equilibrium state was reached in about 400 ms for all samples.

A next important step is the estimation of reliable spin-diffusion coefficients. This was done according to the methods described in Refs. [44,70] and using the mean square distance between the nearest spins estimated in Ref. [44]. The calculated spin-diffusion coefficients for the three components in neat PE and PE/palygorskite nanocomposites are presented in Table 6. Further on, to estimate the size of the domains with different molecular mobility, the spin-diffusion curves were fitted with equations that were obtained using analytical solutions of the spin-diffusion equation for three distinct phases characterized by different spin diffusivities [46]. It should be noted that a 1D spin-diffusion model was assumed in our work, which could be well applied to the lamellae structure identified for molded HDPE samples [44,67,71,72]. Additionally, the lamellae structure was found to be retained in the HDPE/clay nanocomposites as seen by TEM [14].

The extracted thicknesses of three fractions in each sample are shown in Table 6. The NMR long periods, which it is assumed that it can still be calculated as $L = d_C + 2d_i + d_a$ for the nanocomposites as well, are also listed in the last column of the table. Before discussing the effect of fillers on domain sizes, a critical comparison between the lamellae thickness and the long periods that were obtained in our work and the available values reported in the literature is necessary to gauge the reliability of the NMR method. Such an analysis was done with neat PE samples due to the different methods that were applied to study the morphology of high-density polyethylene.

Cheng et al. reported an ^{1}H spin-diffusion measurement based on the decomposition of the ^{13}C spectrum for a linear high-density polyethylene sample ($M_w = 185{,}000$ g/mol, naturally cooled down from the melt). The lamellae thickness of the PE crystallites was shown to be around 26 nm [41]. A determination of lamellae thickness of PE according to the Thomson–Gibbs equation $L_c = \frac{2\sigma T_m^0}{(T_m^0 - T_m)\Delta h_f^0 \rho_c}$ and using the melting peak temperature obtained from the DSC method with a standard heating rate of 10 K/min was reported for both linear and branched polyethylene [71,72]. We therefore calculated the lamellae thickness of the neat PE sample using the related parameters for linear polyethylene reported in the literature [71] (fold surface free energy $\sigma = 93$ mJ/m^2; heat of fusion for a PE sample with 100% crystallinity $\Delta h_f^0 = 293$ J/g, equilibrium melting point for homopolyethylene $T_m^0 = 410$ K, crystal-core density $\rho_c = 1$ g/cm^3). The obtained lamellae thickness of 26 ± 1.3 nm was slightly lower than the NMR lamellae thickness. This is considered reasonable when taking into consideration that the rigid component actually includes the contribution from the crystalline–amorphous interface.

As seen above, the domain sizes extracted from the ^{1}H spin-diffusion experiment at room temperature are in good agreement with literature values. However, neither a quantitative determination of domain sizes in PE/clay nanocomposites nor a discussion on the filler effect has been published to our best knowledge. We thus we believe to present here, for the first time, results of domain sizes and an investigation on the influence of the nanoscale filler. Three points can be extracted from the results in Table 6: 1) Once the nanofiller is introduced, the thickness of the rigid part decreases, and the thickness of interface and amorphous fraction increases. The decrease of the thickness of the rigid phase up to 22% with the introduction of the filler is in agreement with the results found for other filled systems [45]. 2) A further increase of the filler loading leads to a further decrease in the thickness of the rigid fraction, while the thickness of the interface and amorphous fractions increase. 3) Moreover, a decrease of the NMR long period is observed with increasing the amount of filler. A decrease of the long period was also observed for other nanocomposites which showed as well an improvement of the mechanical properties compared with the neat sample [73]. The obtained results indicate that the presence of the filler is affecting not only the crystallization process but also the grow of the rigid lamella.

4. Conclusion

This study shows that the employment of palygorskite as a catalyst carrier and the formation of polyethylene nanocomposites *in situ* during the ethylene polymerization process, represent an attractive route to prepare polyolefins filled with nanoscale silicates. A comparative catalyst activity to solution polymerization can be achieved and, thus, low amounts of a co-catalyst are needed to produce exfoliated nanocomposites. Additionally, the high catalyst activity was obtained without chemical modification of the inorganic clay. The resulting formation of exfoliated nanocomposites was confirmed by TEM and led to a considerable increase in the storage modulus with a filler loading lower than 5 wt.%. It is, therefore, expected that this method can be extended to other types of metallocene catalysts such as Cp_2ZrCl_2 since it is more representative in the family of metallocene catalysts for α-olefin polymerization.

The phase structure of neat PE and PE/clay nanocomposites revealed by solid-state ^{1}H NMR techniques illustrates that phase composition, chain mobility, and domain sizes of polyethylene are affected by the introduction of nanoscale clay fibers and the filler load. Therefore, the filler needs to be carefully examined to evaluate both its impact on the polymer matrix and the final properties of nanocomposites (such as the storage modulus), which are determined by the interplay of the two different effects. This observation gives deeper insight into the structure of nanocomposites and offers the opportunity to set up structure-property relationships as a quantitative analysis of the fine condensed state structure is achieved. Nevertheless, understanding the nanocomposites structure still requires the contribution of more powerful NMR techniques, especially ^{13}C NMR analysis. Work along this line is in progress.

Acknowledgements

Li Wei thanks greatly to the scholarship for the pH.D student from DAAD PPP 2009 funded by CSC. Funding from the project No.

20776124 of Natural Science Foundation of China, the project (No. 20736011) of Natural Science Foundation of China, National High-tech Research Development Program (2007AA030208) and Chinese Universities Scientific Fund are acknowledged.

References

[1] Alexandre M, Dubois P. Mater Sci Eng R 2000;28:1.
[2] Chaiko DJ. E Polymers; 2006:19.
[3] Tanniru M, Yuan Q, Misra RDK. Polymer 2006;47:2133.
[4] Zhao C, Qin H, Gong F, Feng M, Zhang S, Yang M. Polym Degrad Stab 2005;87:183.
[5] Zhang J, Wilkie CA. Polym Degrad Stab 2003;80:163.
[6] Zhang J, Wilkie CA. Polymer 2006;47:5736.
[7] Zhang J, Gupta RK, Wilkie CA. Polymer 2006;47:4537.
[8] Gopakumar TG, Lee JA, Kontopoulou M, Parent JS. Polymer 2002;43:5483.
[9] Wang KH, Xu M, Choi YS, Chung IJ. Polym Bull 2001;46:499.
[10] Wang S, Hu Y, Tang Y, Wang Z, Chen Z, Fan W. J Appl Polym Sci 2003;89:2583.
[11] Tjong SC, Meng YZ. J Polym Sci Part B Polym Phys 2003;41:1476.
[12] Wang KH, Choi MH, Koo CM, Choi YS, Chung IJ. Polymer 2001;42:9819.
[13] Wang KH, Koo CM, Chung IJ. J Appl Polym Sci 2003;89:2131.
[14] Jeon HG, Jung HT, Lee SW, Hudson SD. Polym Bull 1998;41:107.
[15] Kawasumi MJ. Polym Sci Part A Polym Chem 2004;42:819.
[16] Jin YH, Park HJ, Im SS, Kwak SY, Kwak S. Macromol Rapid Commun 2002;23:135.
[17] Yang F, Zhang X, Zhao H, Chen B, Huang B, Feng Z. J Appl Polym Sci 2003;89:3680.
[18] Kuo SW, Huang WJ, Huang SB, Kao HC, Chang FC. Polymer 2003;44:7709.
[19] Lee D, Kim H, Yoon K, Min KE, Seo KH, Noh SK. Sci Technol Adv Mater 2005;6:457.
[20] Wei L, Tang T, Huang B. J Polym Sci Part A Polym Chem 2004;42:941.
[21] Xu JT, Zhao YQ, Wang Q, Fang ZQ. Polymer 2005;46:11978.
[22] Wang J, Liu Z, Guo C, Chen Y, Wang D. Macromol Rapid Commun 2001;22:1422.
[23] Alexandre M, Dubois P, Sun T, Garces JM, Jérôme R. Polymer 2002;43:2123.
[24] Heinemann J, Reichert P, Thomann R, Mülhaupt R. Macromol Rapid Commun 1999;20:423.
[25] Bergman JS, Chen H, Giannelis EP, Thomas MG, Coates GW. Chem Commun; 1999:2179.
[26] Shin SYA, Simon LC, Soares JBP, Scholz G. Polymer 2003;44:5317.
[27] Zheng ZL. Chinese palygorskite minerals. Beijing: Geological Publication Press; 1997.
[28] Yan SH, editor. Clay minerals. Beijing: Geological Publication Press; 1981.
[29] Ando I, Asakura T. Solid state NMR of polymers. Amsterdam: Elsevier Science; 1998.
[30] Schmidt-Rohr K, Spiess HW. Multidimensional solid-state NMR and polymers. London: Academic Press; 1994.
[31] Packer KJ, Pope JM, Yeung RR. J Polym Sci Polym Phys 1984;22:589.
[32] Eckman RR, Henrichs PM, Peacock AJ. Macromolecules 1997;30:2474.
[33] Hansen EW, Kristiansen PE, Pedersen B. J Phys Chem B 1998;102:5444.
[34] Kristiansen PE, Hansen EW, Pedersen B. J Phys Chem B 1999;103:3552.
[35] Uehara H, Yamanobe T, Komoto T. Macromolecules 2000;33:4861.
[36] Hillebrand L, Schmidt A, Bolz A, Hess M, Veeman W. Macromolecules 1998;31:5010.
[37] Flory PJ, Yoon DY, Dill KA. Macromolecules 1984;17:862.
[38] Baker AME, Windle AH. Polymer 2002;42:667.
[39] Ivanov DA, Pop T, Yoon DY, Jonas AM. Macromolecules 2002;35:9813.
[40] Mandelkern L. Macromol Chem 1992;3:347.
[41] Cheng J, Fone M, Reddy VN, Schwartz KB, Fisher HP, Wunderlich B. J Polym Sci Part B Polym Phys 1994;32:2683.
[42] Kidamaru R, Horri F, Zhu Q, Bassett DC, Olley RH. Polymer 1994;35:1171.
[43] Pang W, Fan C, Zhu Q. Eur Polym J 2001;37:2425.
[44] Hedesiu C, Demco D, Kleppinger R, Adams A, Blümich B, Remerie K, et al. Polymer 2007;48:763.
[45] Nowaczyk G, Glowinkowski S, Jurga S. Solid State Nucl Magn Reson 2004;25:194.
[46] Adams-Buda A, Demco D, Bertmer M, Blümich B, Reinig B, Keul H, et al. Solid State Nucl Magn Reson 2003;24:39.
[47] Weir MR, Rutinduka E, Detellier C, Feng CY, Wang Q, Matsuura T, et al. J Membr Sci 2001;182:41.
[48] Taylor JC. Powder Diffraction 1991;6:2.
[49] Massiot D, Fayon F, Capron M, King L, Calvé SL, Alonso B, et al. Magn Reson Chem 2001;40:70.
[50] Adams-Buda A, Demco DE, Blümich B, Litvinov VM, Penning JP. Chem Phys Chem 2004;5:876.
[51] Voda MA, Demco DE, Voda A, Schauber T, Adler M, Dabisch T, et al. Macromolecules 2006;39:4802.
[52] Kaminsky W, Sinn H, editors. Trensition metals and organomatallics für catalyst for olefin polymerisation. New York: Springer; 1998.
[53] Reibeiro MR, Deffieux A, Portela MF. Ind Eng Chem Res 1997;36:1224.
[54] Costa VI, Belelli PG, Santos JHZ, Ferreira ML, Damiani DE. J Catal 2001;204:1.
[55] Lee KS, Oh CG, Yim JH, Ihm SK. J Mol Catal 2000;159:301.
[56] Parry EP. J Catal 1963;2:371.
[57] Hattori H, Shiba T. J Catal 1968;12:111.
[58] Kuang WX, Facey GA, Detellier C, Casal B, Serratosa JM, Hitzky ER. Chem Mater 2003;15:4956.
[59] Finch WC, Gillespie RD, Hedden D, Marks TJ. J Am Chem Soc 1990;112:6221.
[60] Boor J. Ziegler–Natta catalysts and polymerization. New York: Academic Press; 1979.
[61] Wunderlich B. Macromolecular physics. In: Crystal melting, vol. 3. New York: Academic Press; 1980.
[62] McCrum NG. Polyethylene: detailed interpretation of mechanical relaxation in a crystalline polymer. In: Meier DJ, editor. Molecular basis of transition and relaxations. New York: Gordon and Breach; 1978.
[63] Boyer RF. Macromolecules 1973;6:288.
[64] Boyer RF. J Macromol Sci Phys 1973;B8:503.
[65] Matsuoka S, Ispida Y. J Polym Sci 1966;C14:297.
[66] Oven AJ, Ward IM. J Macromol Sci Phys 1973;B7:417.
[67] Neway B, Hedenqvist MS, Gedde UW. Polymer 2003;44:4003.
[68] Vanderhart DL, Asano A, Gilman JW. Chem. Mater 2001;13:3796.
[69] Vanderhart DL, Asano A, Gilman JW. Macromolecules 2001;34:3819.
[70] Demco DE, Johansson A, Tegenfeldt J. Solid State Nucl Magn Reson 1995;4:13.
[71] Hedenqvist M, Angelstok AA, Edsberg L, Larsson PT, Gedde UW. Polymer 1996;37:2887.
[72] Mattozzi A, Neway B, Hedenqvist MS, Gedde UW. Polymer 2005;46:929.
[73] Debowska M, Dolega J, Rudzinska-Girulska J, Piglowski J. Acta Physica Polonica 2008;113:1321–9.

List of abbreviations

CPMAS: Cross-polarization magic-angle spinning
Cp_2TiCl_2: Bis–(cyclopentadienyl)titanium dichloride
D: Spin-diffusion coefficient
d: Domain size
DQ: Double-quantum
DMA: Dynamic mechanical analysis
DTG: Differential thermogravimetry
DSC: Differential scanning calorimetry
FTIR: Fourier transform infrared spectroscopy
HDPE: High-density polyethylene
ICP-AES: Inductively coupled plasma-atomic emission spectroscopy
GPC: Gel permeation chromatography
MAO: Methylaluminoxane
MQ: Multiple-quantum
NC: Nascent nanocomposite
NMR: Solid-state nuclear magnetic resonance
PE: Polyethylene
PLT: Palygorskite
SAXS: Small-angle X-ray scattering
SEM: Scanning electron microscopy
T_1: Longitudinal magnetization relaxation
TEM: Transmission electron microscopy
T_g: Glass temperature
T_m: Melting temperature
TIBA: Triisobutylaluminium
TG: Thermogravimetry
XRD: X-ray diffraction
SAXS: Small-angle X-ray scattering
WAXD: Wide angle X-ray diffraction